Diverse roles of the metal binding domains and transport mechanism of copper transporting P-type ATPases

Zongxin Guo[a], Fredrik Orädd[b], Viktoria Bågenholm[a], Christina Grønberg[a], Jian Feng Ma[c], Peter Ott[d], Yong Wang[e], Magnus Andersson[b], Per Amstrup Pedersen[f], Kaituo Wang[a, #,†] & Pontus Gourdon[a,g,†]

[a] Department of Biomedical Sciences, Copenhagen University, Copenhagen, Denmark
[b] Department of Chemistry, Umeå University, Umeå, Sweden
[c] Institute of Plant Science and Resources, Okayama University, Japan
[d] Medical Department of Hepatology and Gastroenterology, Aarhus University Hospital, Skejby, Denmark
[e] College of Life Sciences, Zhejiang University, Zhejiang, China
[f] Department of Biology, University of Copenhagen, Copenhagen, Denmark
[g] Department of Experimental Medical Science, Lund University, Lund, Sweden
[#] Current address: State Key Laboratory of Plant Diversity and Specialty Crops, Institute of Botany, Chinese Academy of Sciences, Beijing, China
[†] Correspondence should be addressed to: K.W. (kaituo@sund.ku.dk) or P.G. (pontus@sund.ku.dk)

Supplementary figure 1

a

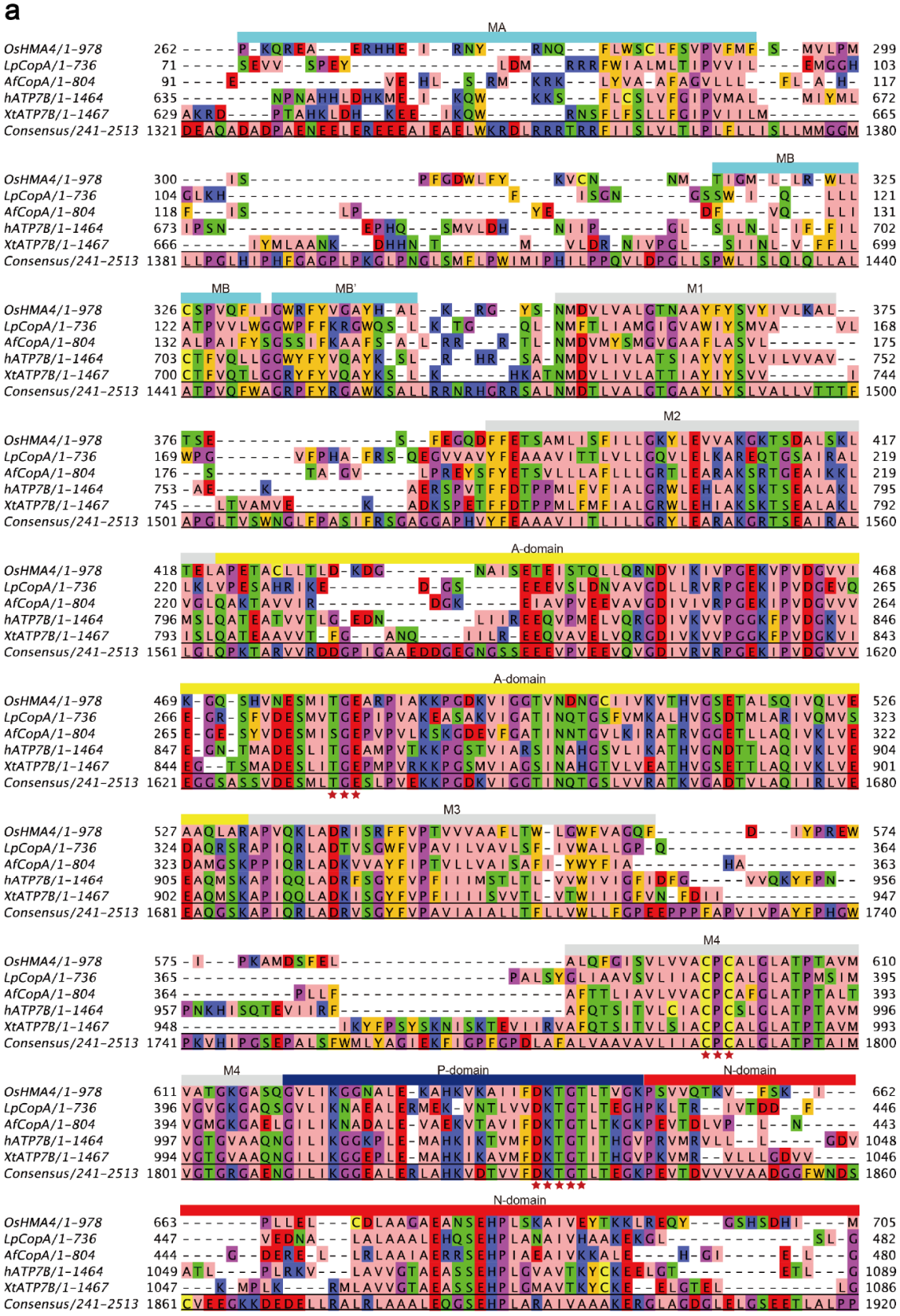

a

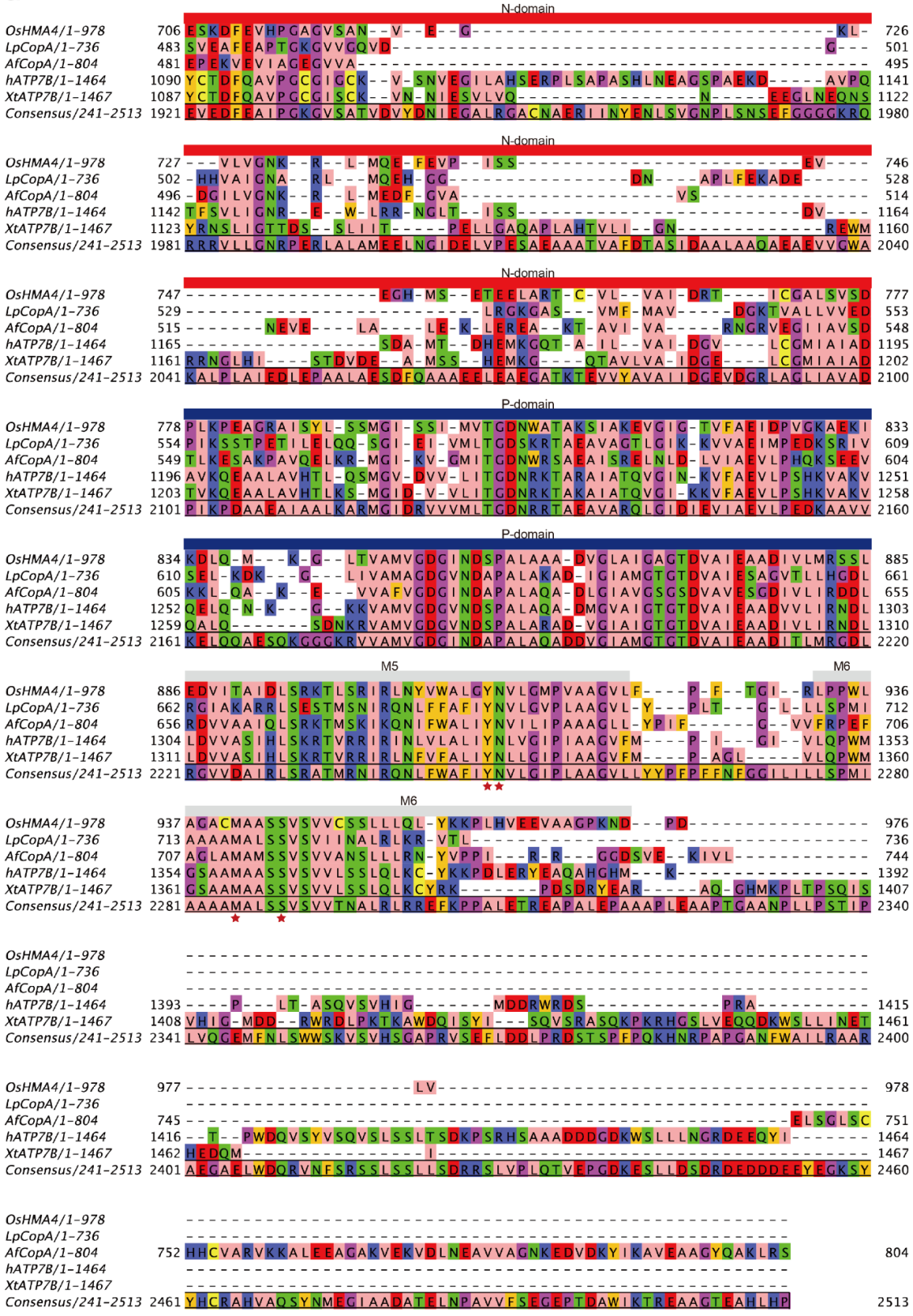
N-domain
OsHMA4/1-978 706 ESKDFEVHPGAGVSAN--V--E--G-------------------------------KL- 726
LpCopA/1-736 483 SVEAFEAPTGKGVVGQVD-------------------------------------G--- 501
AfCopA/1-804 481 EPEKVEVIAGEGVVA-- 495
hATP7B/1-1464 1090 YCTDFQAVPGCGISCK--V-SNVEGILAHSERPLSAPASHLNEAGSPAEKD-----AVPQ 1141
XtATP7B/1-1467 1087 YCTDFQAVPGCGISCK--VN-NIESVLVQ----------------N-----EEGLNEQNS 1122
Consensus/241-2513 1921 FVEDFEAIPGKGVSATVDVYDNIFGALRGACNAFRIINYFNLSVGNPLSNSFFGGGGKRQ 1980
N-domain
OsHMA4/1-978 727 ---VLVGNK--R--L-MQE-FEVP--ISS-------------------------EV---- 746
LpCopA/1-736 502 -HHVAIGNA--RL--MQEH-GG----------------DN----APLFEKADE------ 528
AfCopA/1-804 496 -DGILVGNK--R--L-MEDF-GVA----------------VS---------------- 514
hATP7B/1-1464 1142 TFSVLIGNR--E--W-LRR-NGLT--ISS-------------------------DV---- 1164
XtATP7B/1-1467 1123 YRNSLIGTTDS--SLIIT-----PELLGAQAPLAHTVLI--GN-------------REWM 1160
Consensus/241-2513 1981 RRRVLLGNRPERLALAMEELNGIDELVPESAFEAAATVAFDTASIDAALAAQAFEAFVVGWA 2040
N-domain
OsHMA4/1-978 747 ----------------EGH-MS--ETEELART-C-VL--VAI-DRT----ICGALSVSD 777
LpCopA/1-736 529 ----------------------LRGKGAS---VMF-MAV-----DGKTVALLVVED 553
AfCopA/1-804 515 -------NEVE----LA----LE-K-LEREA--KT-AVI-VA-----RNGRVEGIIAVSD 548
hATP7B/1-1464 1165 ----------------SDA-MT--DHEMKGQT-A-IL--VAI-DGV-----LCGMIAIAD 1195
XtATP7B/1-1467 1161 RRNGLHI----STDVDE--A-MSS--HEMKG----QTAVLVA-IDGE----LCGMIAIAD 1202
Consensus/241-2513 2041 KALPLAIEDLEPAALAESDFQAAAEELEAEGATKTEVVYAVAIIDGEVDGRLAGLIAVAD 2100
P-domain
OsHMA4/1-978 778 PLKPEAGRAISYL-SSMGI-SSI-MVTGDNWATAKSIAKEVGIG-TVFAEIDPVGKAEKI 833
LpCopA/1-736 554 PIKSSTPETILELQQ-SGI-EI-VMLTGDSKRTAEAVAGTLGIK-KVVAEIMPEDKSRIV 609
AfCopA/1-804 549 TLKESAKPAVQELKR-MGI-KV-GMITGDNWRSAEAISRELNLD-LVIAEVLPHQKSEEV 604
hATP7B/1-1464 1196 AVKQEAALAVHTL-QSMGV-DVV-LITGDNRKTARAIATQVGIN-KVFAEVLPSHKVAKV 1251
XtATP7B/1-1467 1203 TVKQEAALAVHTLKS-MGID-V-VLITGDNRKTAKAIATQVGI-KKVFAEVLPSHKVAKV 1258
Consensus/241-2513 2101 PIKPDAAFAIAALKARMGIDRVVVMLTGDNRRTAFAVARQLGIDIFVIAFVLPFDKAAVV 2160
P-domain
OsHMA4/1-978 834 KDLQ-M---K-G--LTVAMVGDGINDSPALAAA-DVGLAIGAGTDVAIEAADIVLMRSSL 885
LpCopA/1-736 610 SEL-KDK---G---LIVAMAGDGVNDAPALAKAD-IGIAMGTGTDVAIESAGVTLLHGDL 661
AfCopA/1-804 605 KKL-QA--K--E---VVAFVGDGINDAPALAQA-DLGIAVGSGSDVAVESGDIVLIRDDL 655
hATP7B/1-1464 1252 QELQ-N-K---G--KKVAMVGDGVNDSPALAQA-DMGVAIGTGTDVAIEAADVVLIRNDL 1303
XtATP7B/1-1467 1259 QALQ-------SDNKRVAMVGDGVNDSPALARAD-VGIAIGTGTDVAIEAADIVLIRNDL 1310
Consensus/241-2513 2161 KELQQAFSQKGGGKRVVAMVGDGINDAPALAQADDVGIAMGTGTDVAIEAADITLMRGDL 2220
M5
M6
OsHMA4/1-978 886 EDVITAIDLSRKTLSRIRLNYVWALGYNVLGMPVAAGVLF----P-F--TGI--RLPPWL 936
LpCopA/1-736 662 RGIAKARRLSESTMSNIRQNLFFAFIYNVLGVPLAAGVL-Y---PLT---G-L-LLSPMI 712
AfCopA/1-804 656 RDVVAAIQLSRKTMSKIKQNIFWALIYNVILIPAAAGLL-YPIF------G--VVFRPEF 706
hATP7B/1-1464 1304 LDVVASIHLSKRTVRRIRLNFVFALIYNLLGIPIAAGVFM----P-I---GI--VLQPWM 1353
XtATP7B/1-1467 1311 LDVVASIHLSKRTVRRIRLNFVFALIYNLLGIPIAAGVFM----P-AGL-----VLQPWM 1360
Consensus/241-2513 2221 RGVVDAIRLSRATMRNIRQNLFWAFIYNVLGIPLAAGVLLYYPFPFFNFGGILILLSPMI 2280
M6
OsHMA4/1-978 937 AGACMAASSVSVVCSSLLLQL-YKKPLHVEEVAAGPKND---PD---------------- 976
LpCopA/1-736 713 AAAAMALSSVSVIINALRLKR-VTL---------------------------------- 736
AfCopA/1-804 707 AGLAMAMSSVSVVANSLLLRN-YVPPI---R-R---GGDSVE--KIVL---------- 744
hATP7B/1-1464 1354 GSAAMAASSVSVVLSSLQLKC-YKKPDLERYEAQAHGHM---K---------------- 1392
XtATP7B/1-1467 1361 GSAAMAASSVSVVLSSLQLKCYRK--------PDSDRYEAR-----AQ-GHMKPLTPSQIS 1407
Consensus/241-2513 2281 AAAAMALSSVSVVTNALRLRREFKPPALETREAPALEPAAAPLEAAPTGAANPLLPSTIP 2340
OsHMA4/1-978 ----------
LpCopA/1-736 ----------
AfCopA/1-804 ----------
hATP7B/1-1464 1393 ----P---LT-ASQVSVHIG--------MDDRWRDS----------PRA---------- 1415
XtATP7B/1-1467 1408 VHIG-MDD--RWRDLPKTKAWDQISYI---SQVSRASQKPKRHGSLVEQQDKWSLLINET 1461
Consensus/241-2513 2341 LVQGEMFNLSWWSKVSVHSGAPRVSEFLDDLPRDSTSPFPQKHNRPAPGANFWAILRAAR 2400
OsHMA4/1-978 977 ----------LV---------- 978
LpCopA/1-736 ----------
AfCopA/1-804 745 ----------ELSGLSC 751
hATP7B/1-1464 1416 --T--PWDQVSYVSQVSLSSLTSDKPSRHSAAADDDGDKWSLLLNGRDEEQYI-------- 1464
XtATP7B/1-1467 1462 HEDQM----------I---------- 1467
Consensus/241-2513 2401 AEGAELWDQRVNFSRSSLSSLLSDRRSLVPLQTVEPGDKESLLDSDRDEDDDEEYEGKSY 2460
OsHMA4/1-978 ----------
LpCopA/1-736 ----------
AfCopA/1-804 752 HHCVARVKKALEEAGAKVEKVDLNEAVVAGNKEDVDKYIKAVEEAAGYQAKLRS 804
hATP7B/1-1464 ----------
XtATP7B/1-1467 ----------
Consensus/241-2513 2461 YHCRAHVAQSYNMEGIAADATELNPAVVFSEGEPTDAWIKTREAAGTEAHLHP 2513

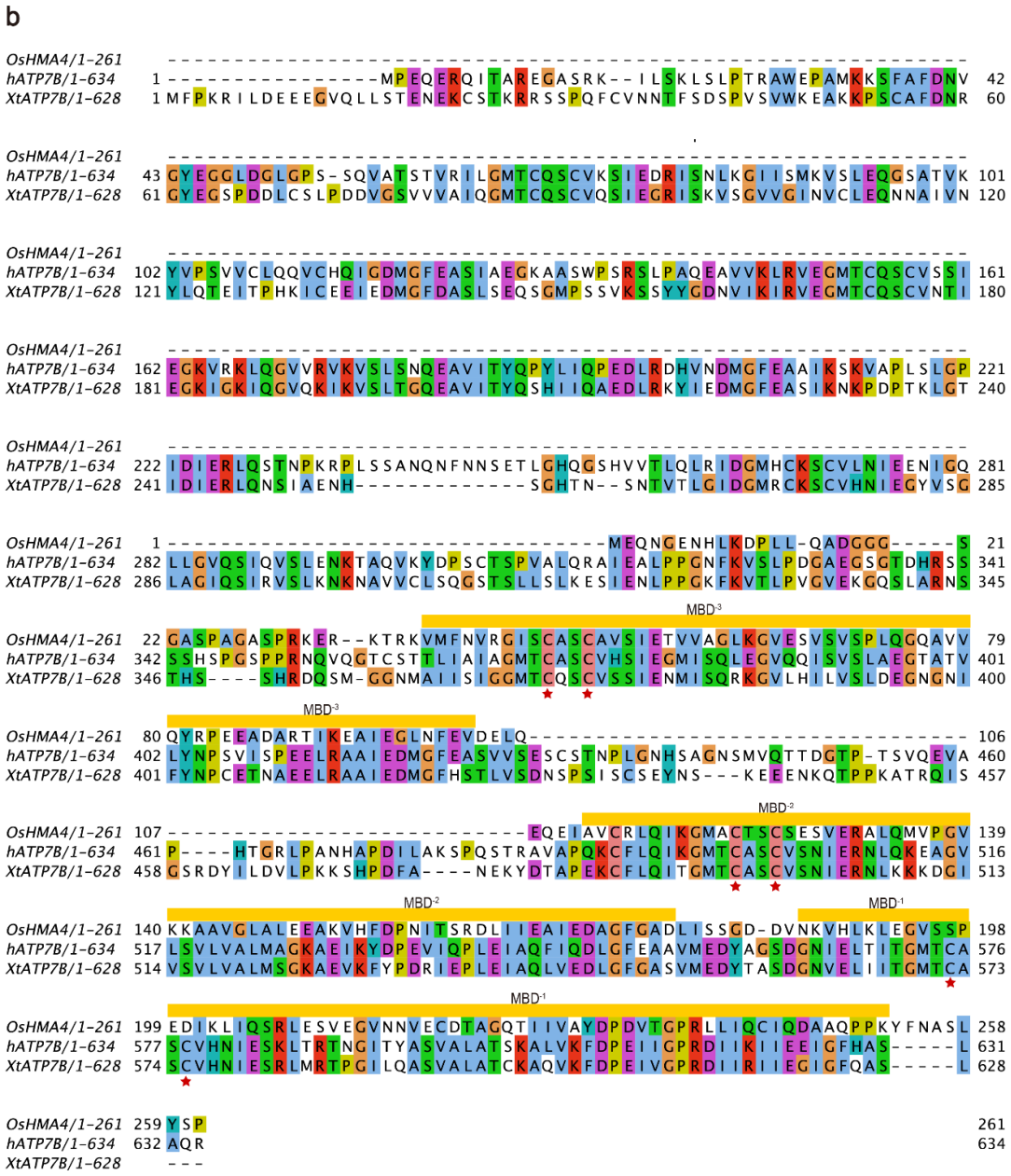

Supplementary figure 1: Conserved sequence features among P_{1B-1}-ATPases. Sequence alignment of copper-transporting P-type ATPases (all containing the CPC motif in M4, DKTGT in the P-domain, YN in M5, and MXXSS in M6 - motifs associated with Cu^{+}/Ag^{+} pumps). Alignments were performed using Clustal Omega and visualized using Jalview. Relevant structural features are highlighted above the sequences. **a,** Alignment of *Oryza sativa* HMA4 (Q6H7M3), *Legionella pneumophila* CopA (Q5ZWR1), Archaeoglobus fulgidus CopA (O29777), human ATP7B (P35670) and *Xenopus tropicalis* ATP7B (A0A6I8R0A5) and the consensus of 1713 CopA proteins, spanning from the MA until the C-terminus (the N-termini have been removed for clarity). **b,** Alignment of the N-termini (until MA) of HMA4, hATP7B and XtATP7B.

Supplementary figure 2

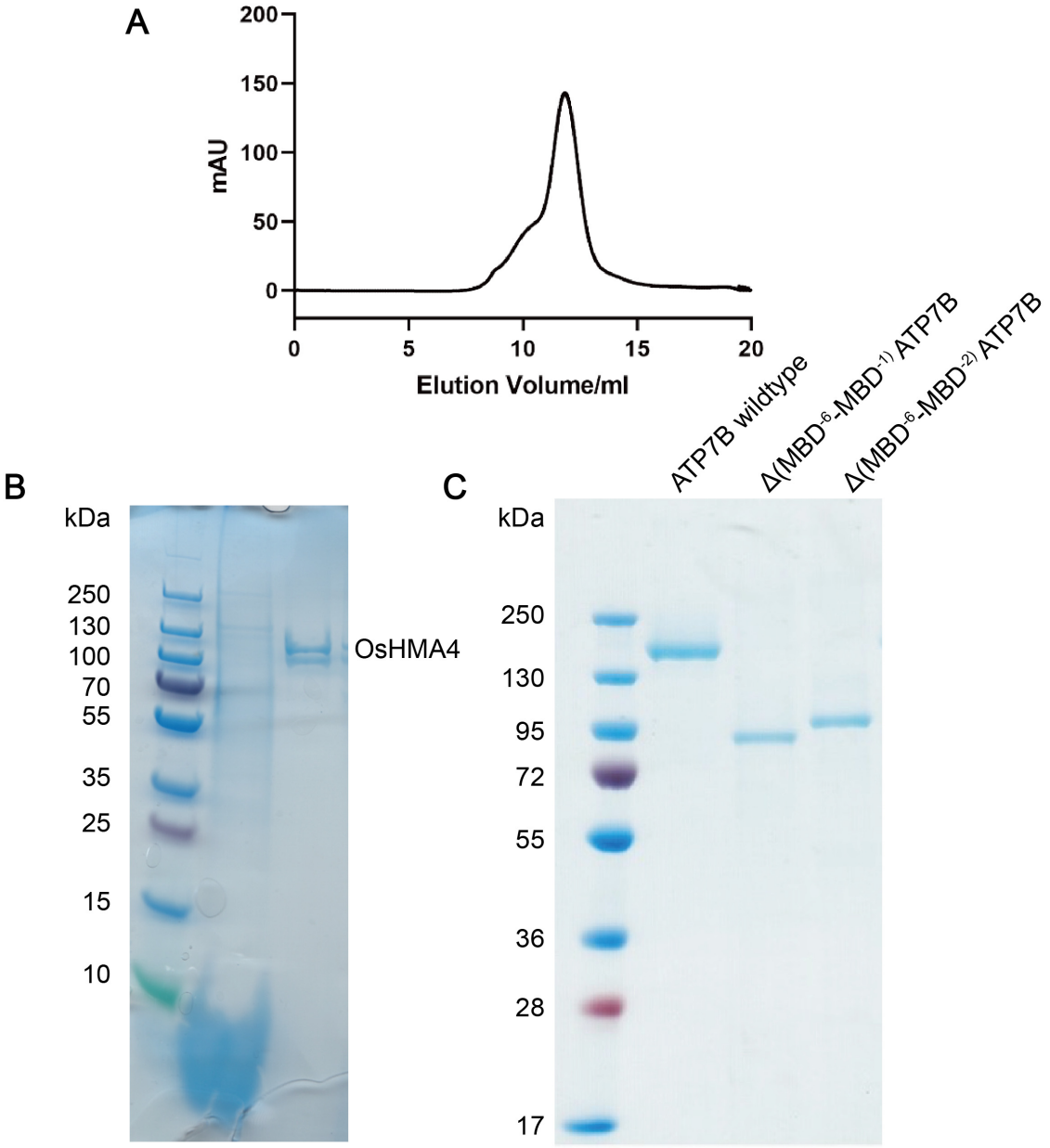

Supplementary figure 2: *Oryza sativa* HMA4 and human ATP7B sample quality as recovered from *Saccharomyces cerevisiae*. a, The size-exclusion chromatography profile following purification of HMA4. **b,** SDS-PAGE analysis of HMA4 following size-exclusion chromatography of HMA4. An unrelated sample is present in the well in-between the markers and OsHMA4. **c,** SDS-PAGE analysis of human ATP7B.

Supplementary figure 3

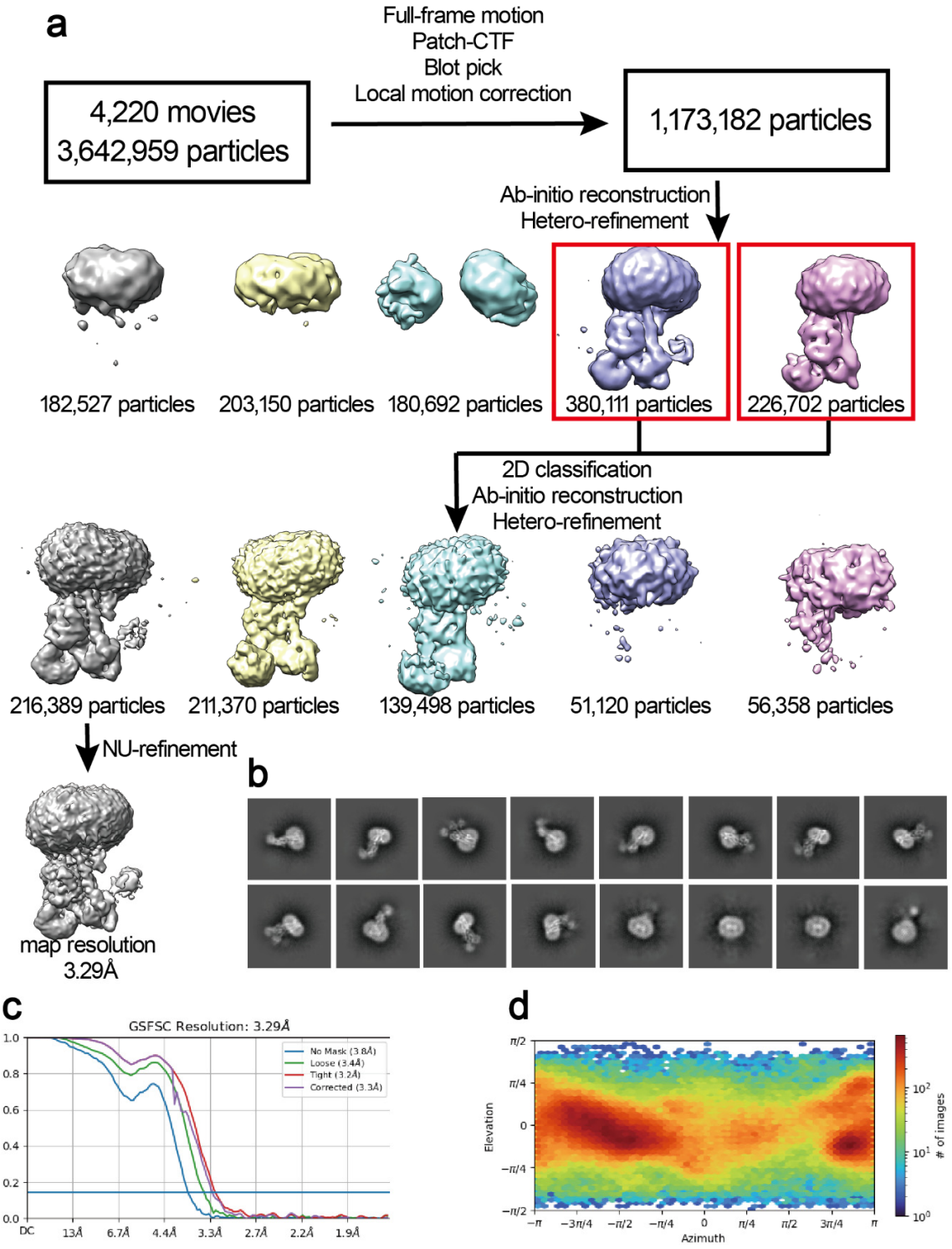

Supplementary figure 3: Data processing of the HMA4^{BeF} structure (E2P state). a, Data processing flowchart. **b,** Representative 2D class averages. The box size was 30 nm. **c,** Gold standard Fourier shell correlation (FSC) curve of the final map. **d,** Particle orientation distributions in the final 3D reconstruction.

Supplementary figure 4

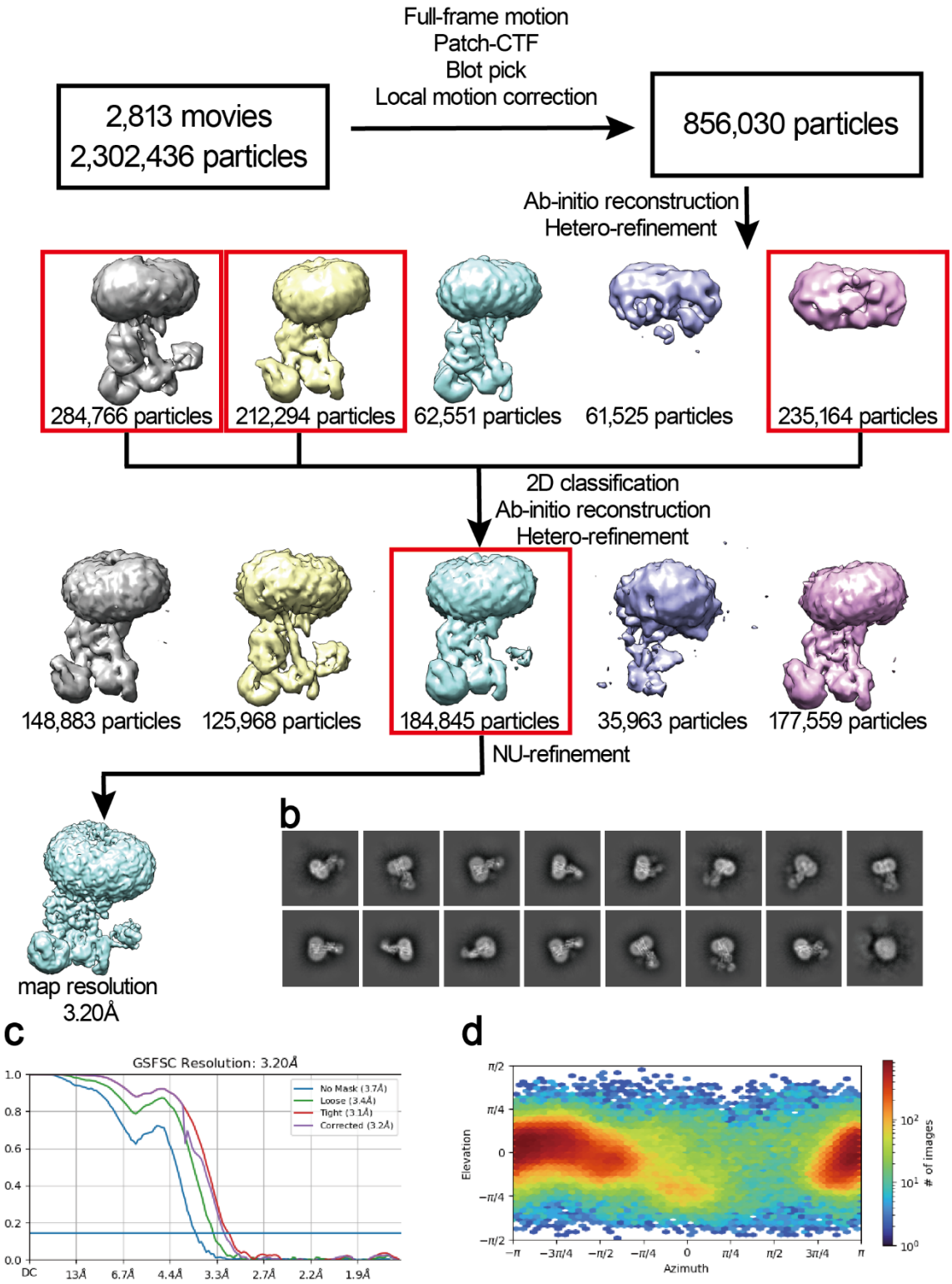

Supplementary figure 4: Data processing of the HMA4^{AlF} structure (E2P state). a, Data processing flowchart. **b,** Representative 2D class averages. The box size was 30 nm. **c,** Gold standard Fourier shell correlation (FSC) curve of the final map. **d,** Particle orientation distributions in the final 3D reconstruction.

Supplementary figure 5

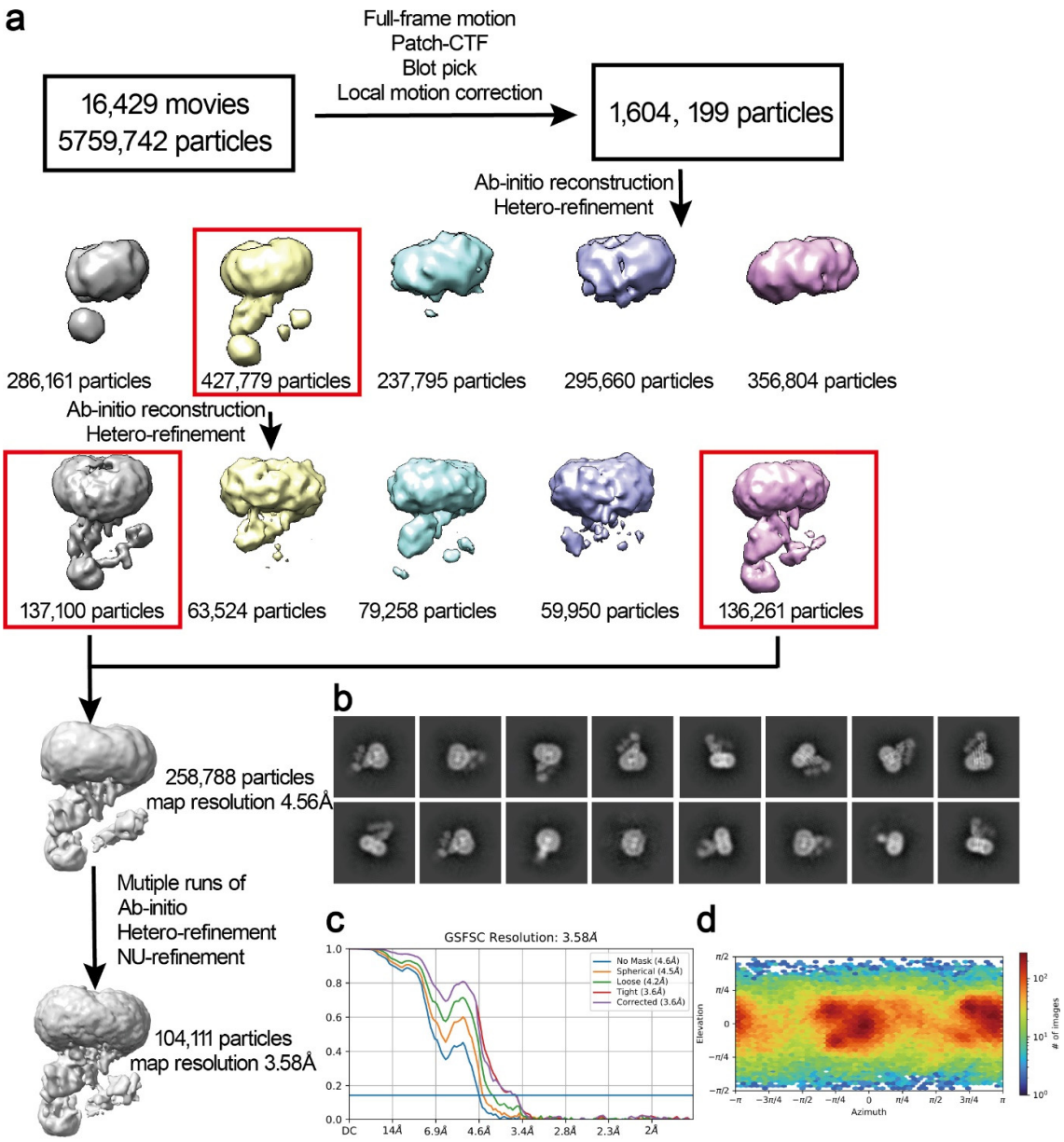

Supplementary figure 5: Data processing of the HMA4^{apo} structure (E1 state). a, Data processing flowchart. **b,** Representative 2D class averages. The box size was 30 nm. **c,** Gold standard Fourier shell correlation (FSC) curve of the final map. **d,** Particle orientation distributions in the final 3D reconstruction.

Supplementary figure 6

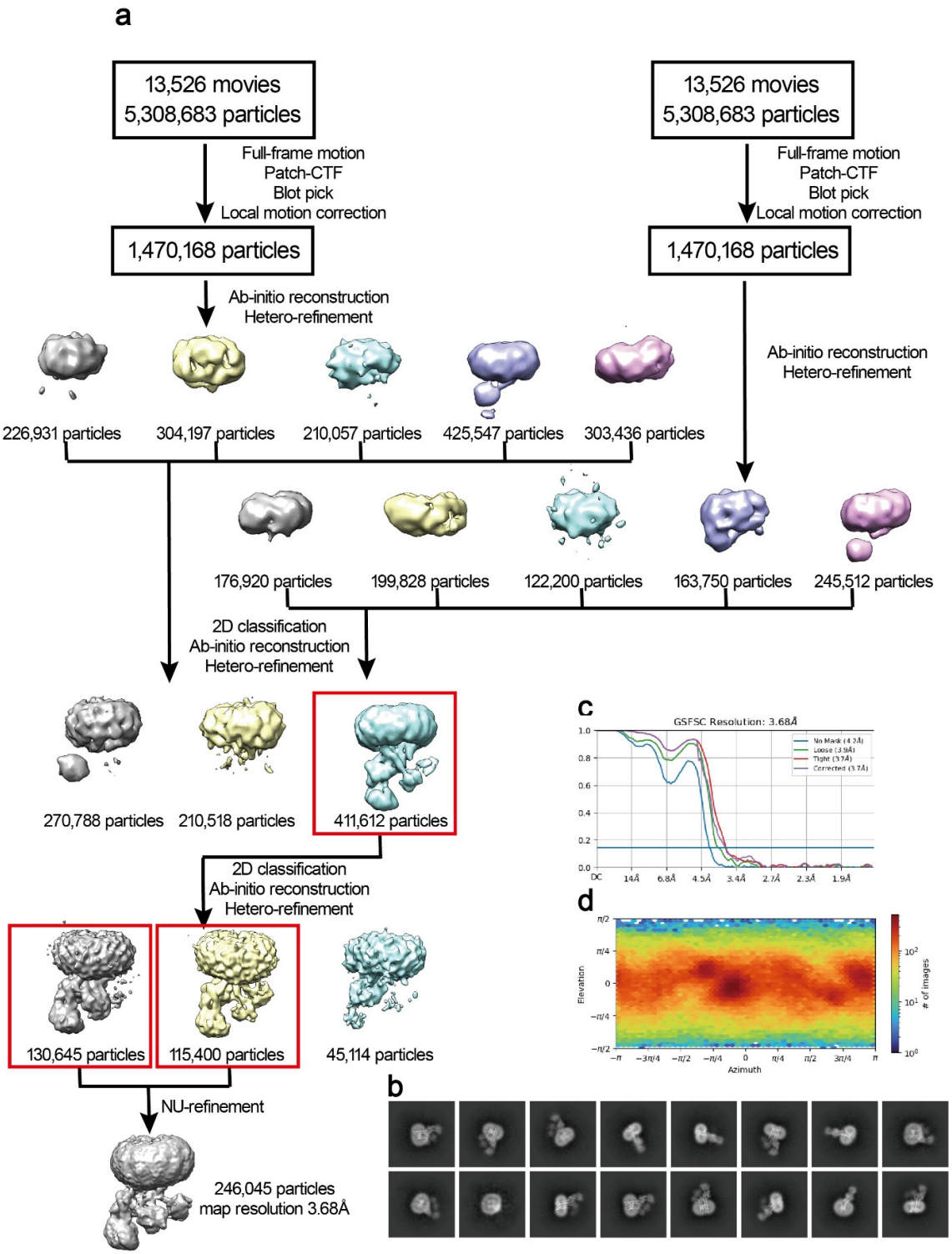

Supplementary figure 6: Data processing of the HMA4^{Cu} structure (E1-Cu state). a, Data processing flowchart. **b,** Representative 2D class averages. The box size was 30 nm. **c,** Gold standard Fourier shell correlation (FSC) curve of the final map. **d,** Particle orientation distributions in the final 3D reconstruction.

Supplementary figure 7

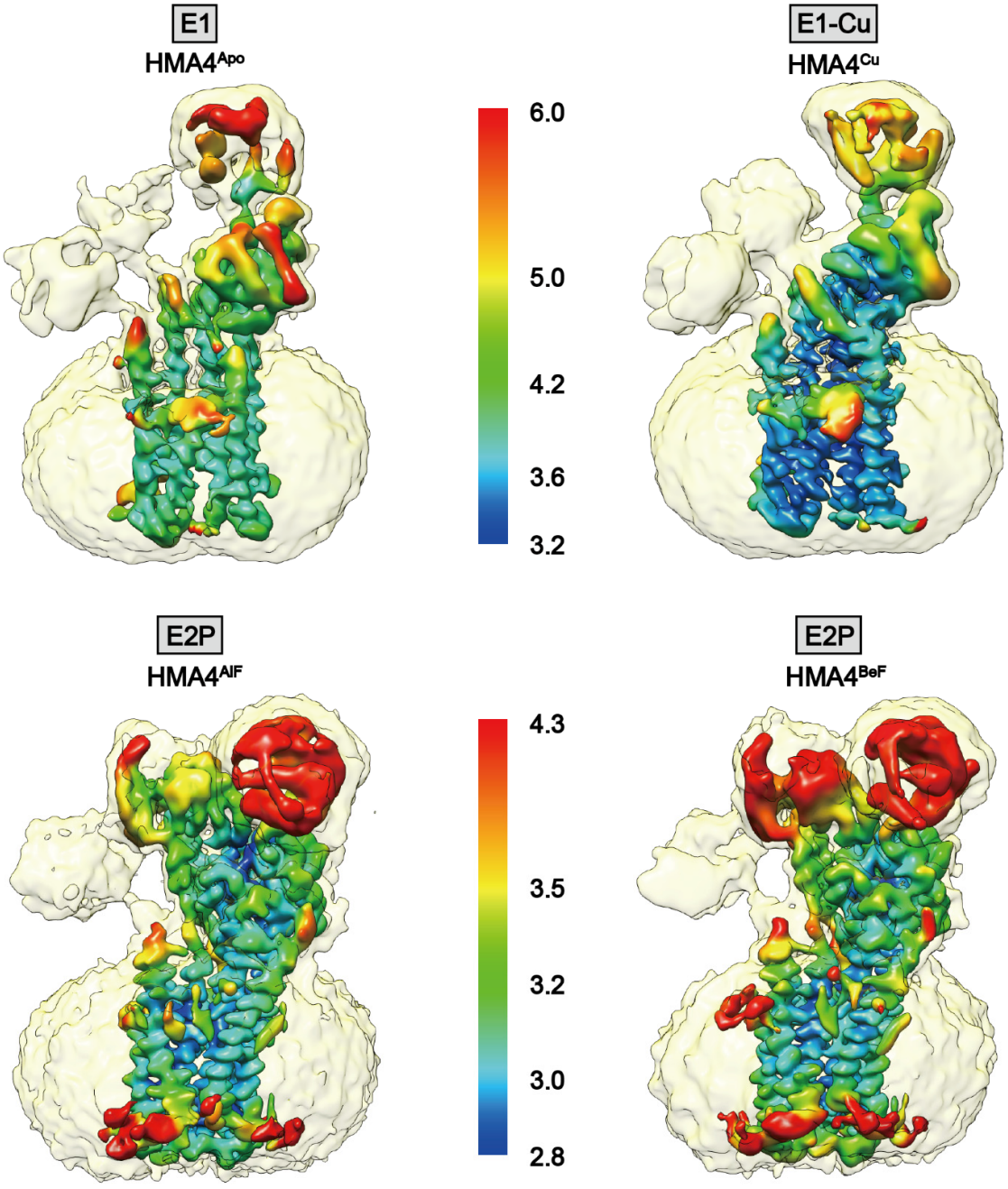

Supplementary figure 7: Local resolution of the cryo-EM maps of the generated HMA4 structures.

Supplementary figure 8

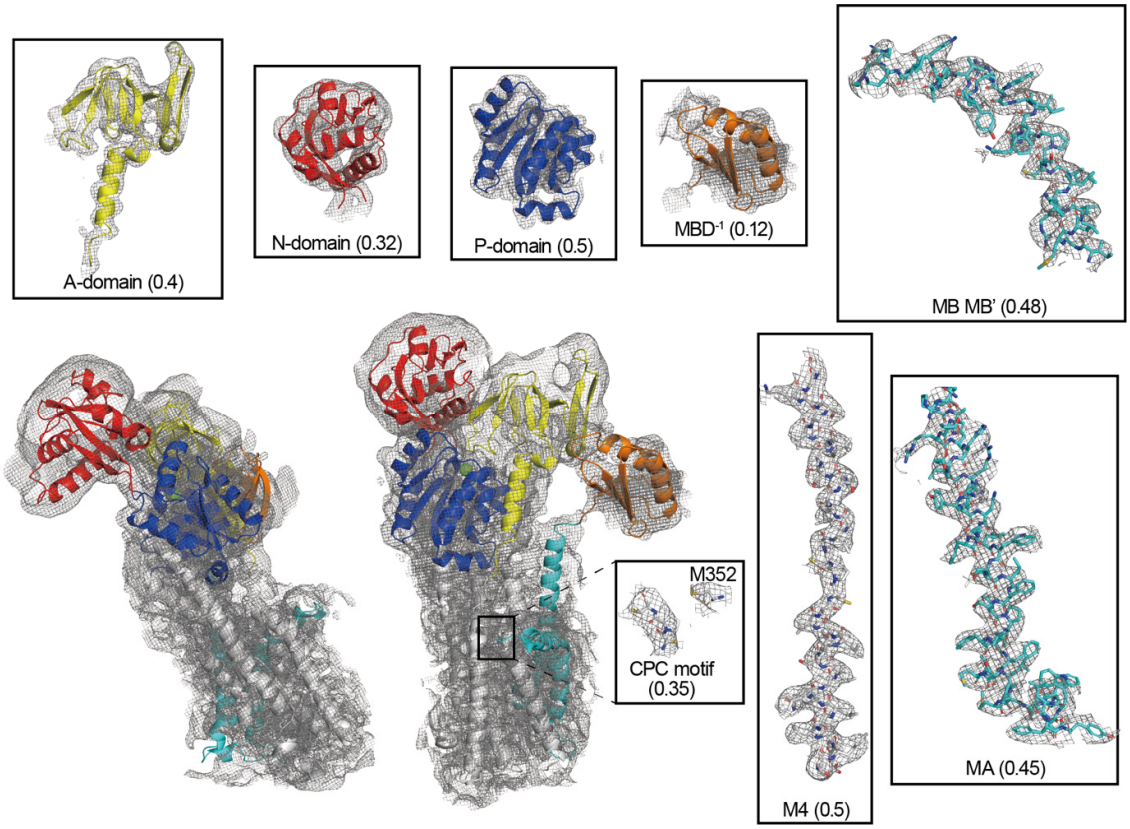

Supplementary figure 8: Cryo-EM map quality of the HMA4^{BeF} structure (E2P state). The protein parts of colored as in Fig. 1. Contour levels are indicated in brackets.

Supplementary figure 9

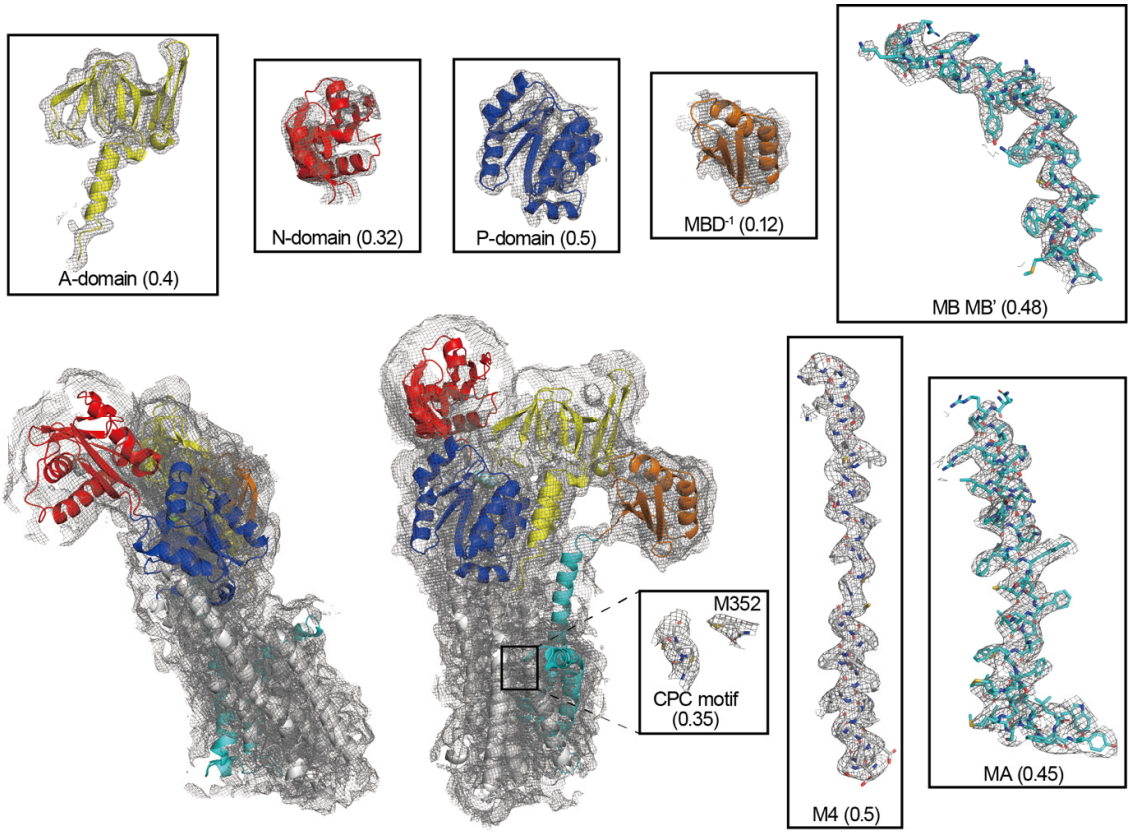

Supplementary figure 9: Cryo-EM map quality of the HMA4^{AlF} structure (E2P state). The protein parts of colored as in Fig. 1. Contour levels are indicated in brackets.

Supplementary figure 10

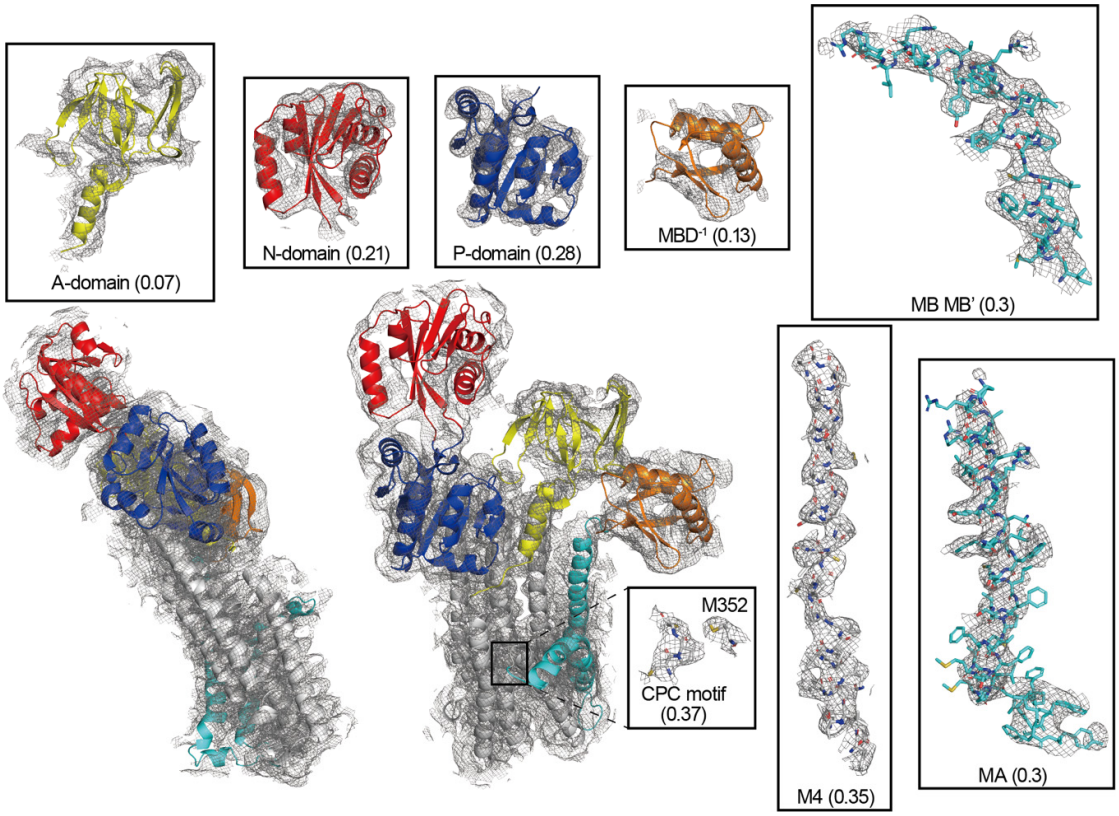

Supplementary figure 10: Cryo-EM map quality of the HMA4^{apo} structure (E1 state). The protein parts of colored as in Fig. 1. Contour levels are indicated in brackets.

Supplementary figure 11

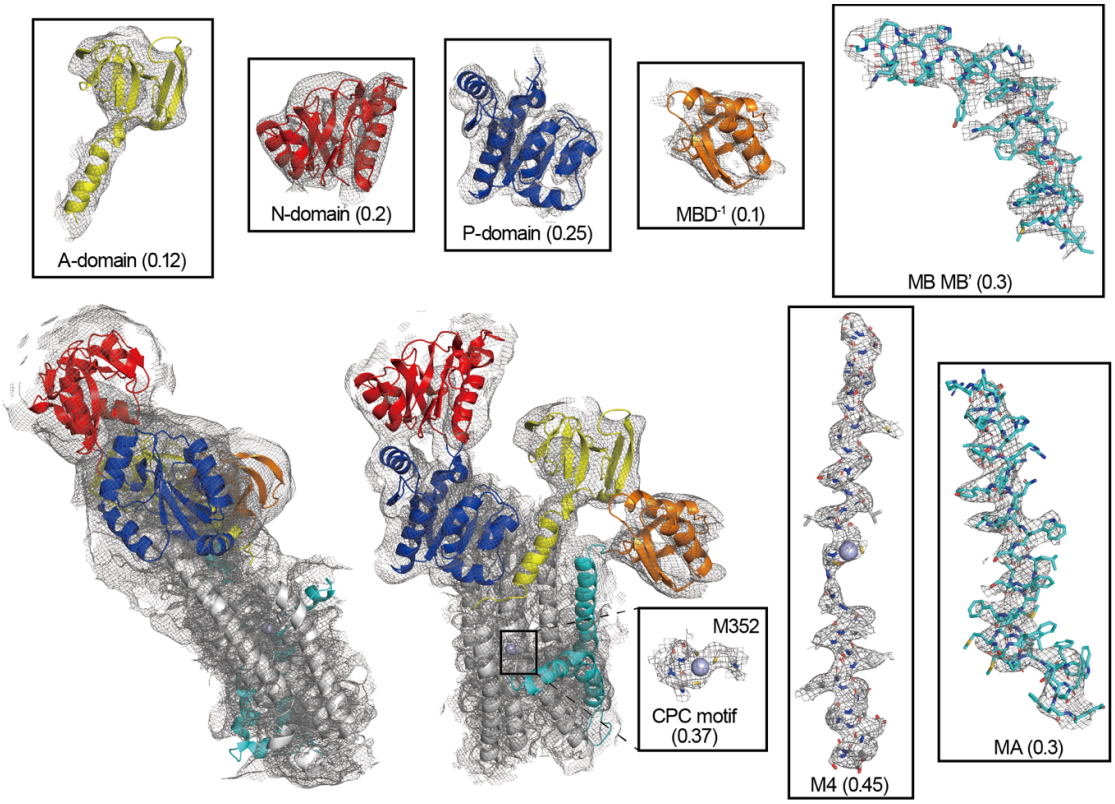

Supplementary figure 11: Cryo-EM map quality of the HMA4^{Cu} structure (E1-Cu state). The protein parts of colored as in Fig. 1. Contour levels are indicated in brackets.

Supplementary figure 12

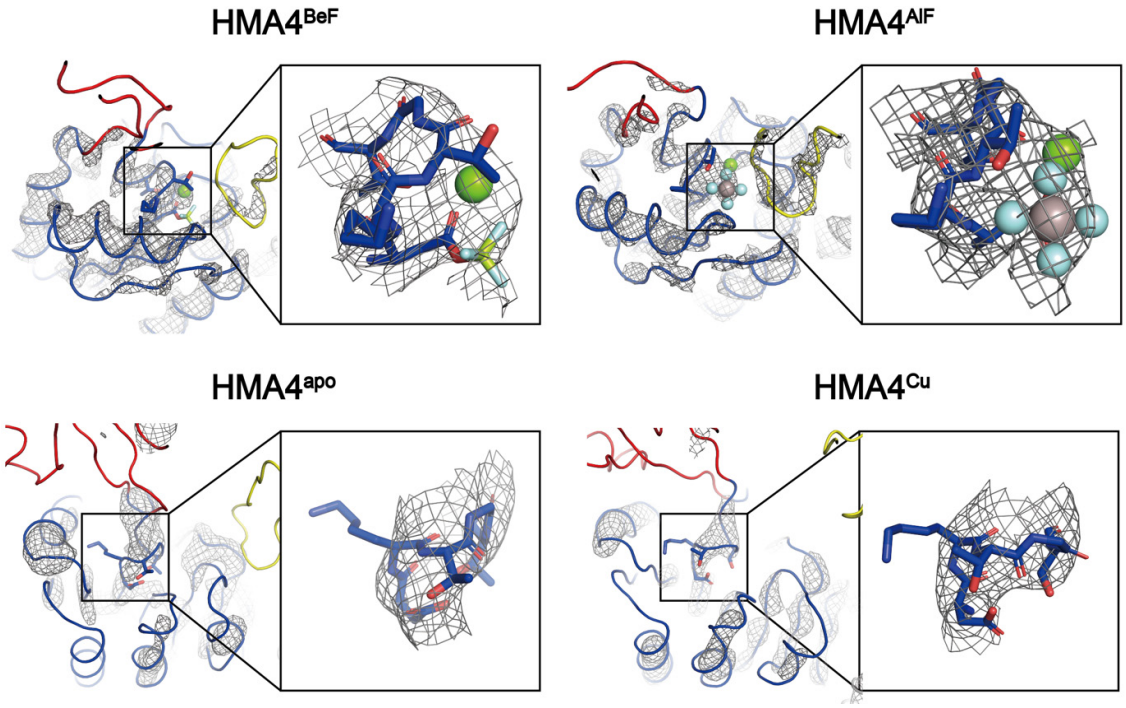

Supplementary figure 12: The DKTGT-regions in the determined HMA4 structures. Note that the density is shown at high signal-to-noise level where even some secondary structure is missing, and yet support for the phosphate mimics is present in $HMA4^{BeF}$ and $HMA4^{AlF}$, respectively.

Supplementary figure 13

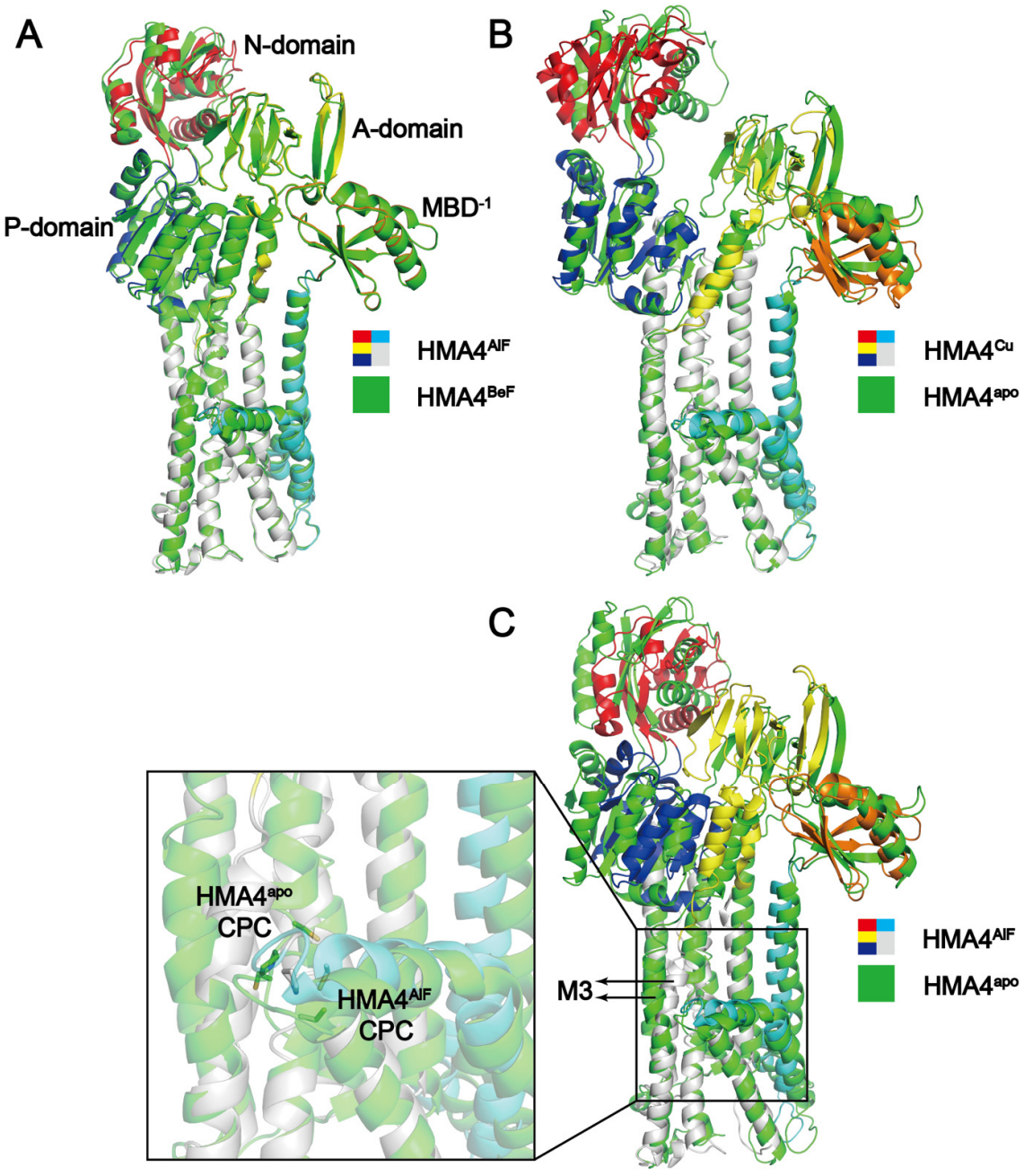

Supplementary figure 13: Structural comparisons of the determined HMA4 structures. Structures were aligned using super in Pymol and using the complete structures. **a,** $HMA4^{AlF}$ versus $HMA4^{BeF}$. **b,** $HMA4^{Cu}$ versus $HMA4^{apo}$. **c,** $HMA4^{AlF}$ versus $HMA4^{apo}$, including a close-view of the CPC-motif showing the CPC-motif is more surface-exposed in $HMA4^{apo}$ than in $HMA4^{ALF}$.

Supplementary figure 14

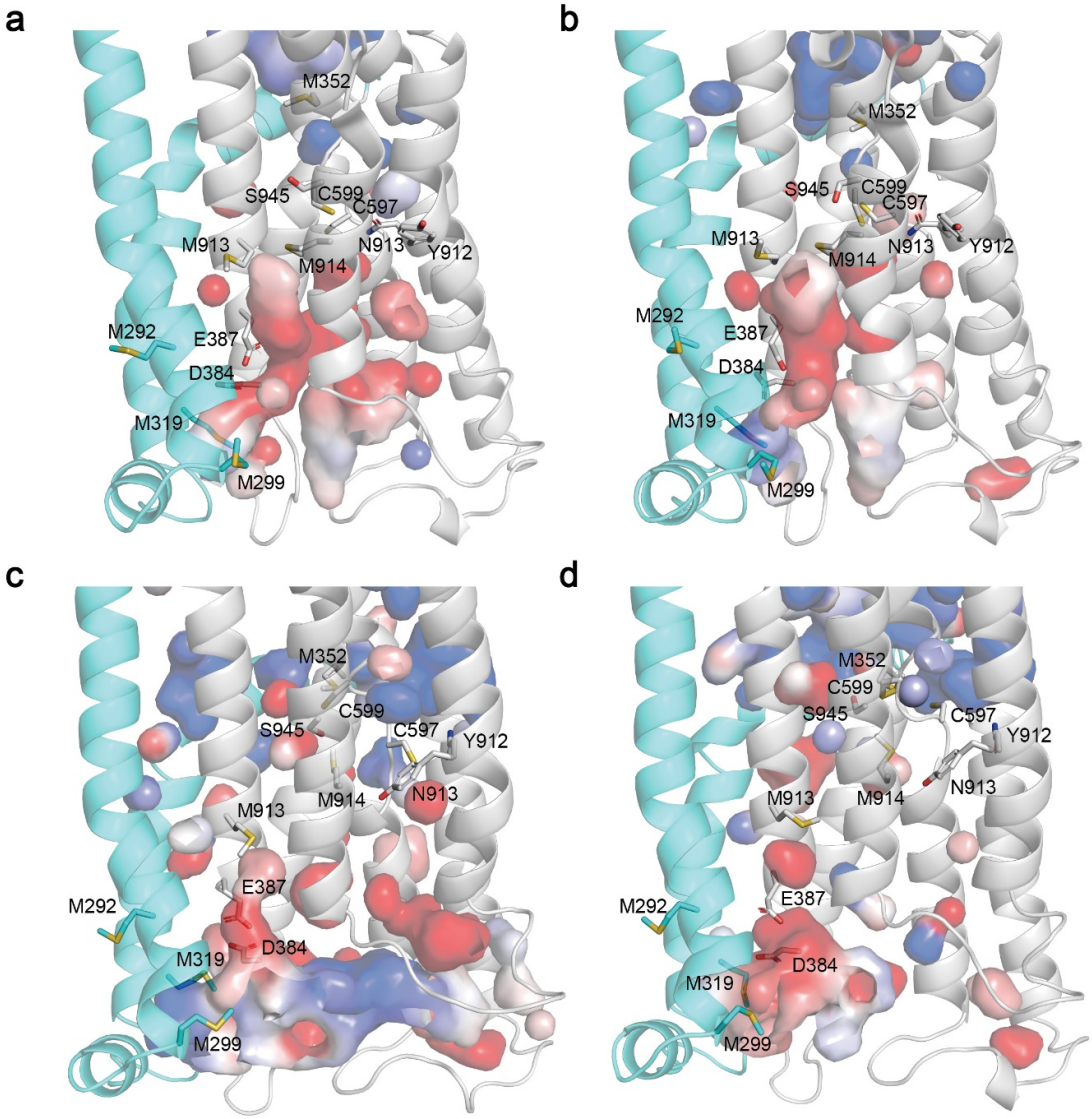

Supplementary figure 14: Surface analyses of HMA4, with access from the extracellular side to the residues contributing to the high-affinity binding site in the E2P, but not the E1 states. a, $HMA4^{BeF}$; **b**, HMA^{AlF}; **c,** HMA^{apo}; **d,** HMA^{Cu}.

Supplementary figure 15

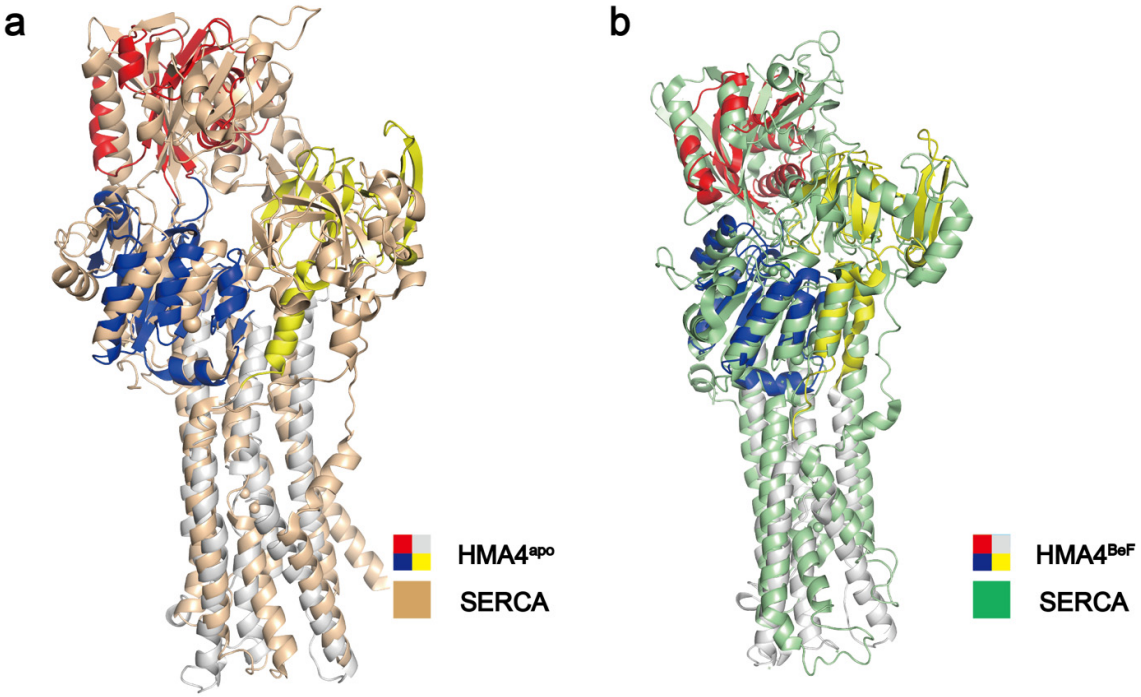

Supplementary figure 15: Structural comparisons of selected HMA4 structures to SERCA. a, Structural comparison of $HMA4^{Cu}$ and SERCA (PDB 4H1W). **b,** structural comparison of $HMA4^{AlF}$ and SERCA (PDB-ID 3B9B). The alignment was conducted using super in Pymol and using the complete structures. For clarity, the MBD, MA and MB as well as M7-M10 have been removed in HMA4 and SERCA, respectively.

Supplementary figure 16

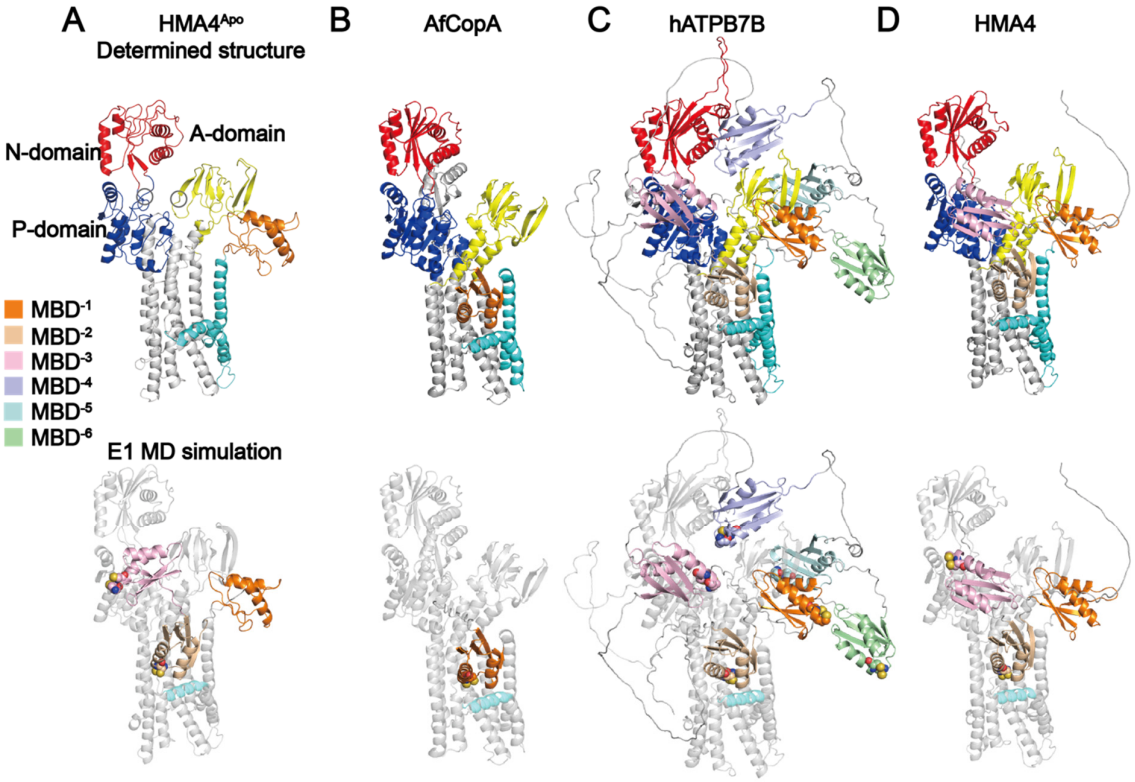

Supplementary figure 16: Comparisons between HMA4^{apo} and AlphaFold structures A, Overview of different P_{IB-I} AlphaFold models, as aligned in PyMol to HMA4^{apo}. Top are overviews of the structures, coloured as in Fig. 1a. Bottom are the same views, but with the core faded out, highlighting the MBDs. The structures shown are HMA4^{apo} (A, including MBDs from the MD simulation in the bottom view), and AlphaFold models of AfCopA (B), hATB7B (C) and HMA4 (D). The MBDs are colored as shown on the left.

Supplementary figure 17

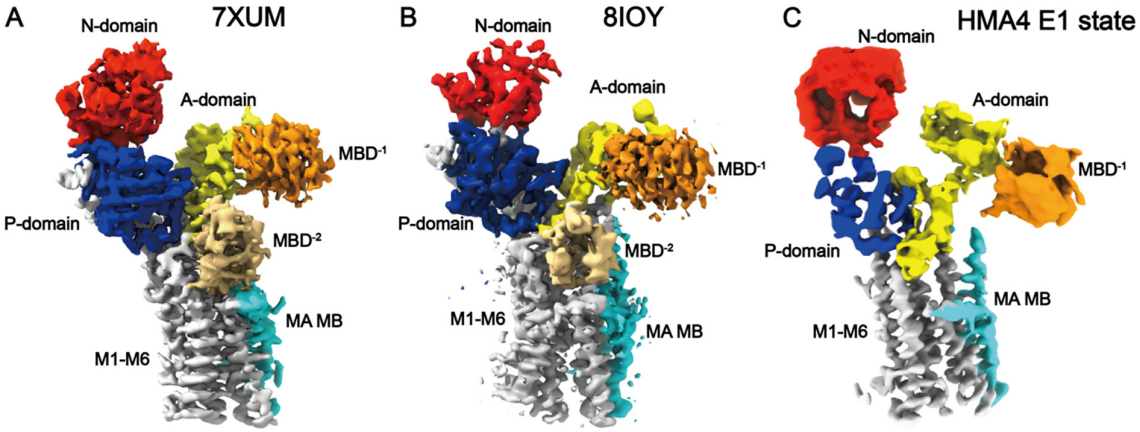

Supplementary figure 17: The previously determined structures of human ATP7B, compared to HMA^{apo}. Density maps of the previously determined structure of human ATP7B (PDB-IDs A: 7XUM B: 8IOY), as well as HMA^{apo} (C). Density of the N-domain in red, P-domain in blue, MA-MB in cyan and M1-M6 in gray. The wheat density was previously assigned as MBD^{-1} while the orange density was left unassigned. We expect the orange density represents MBD^{-1} (as shown in this manuscript), while the wheat density corresponds to MBD^{-2}.

Supplementary figure 18

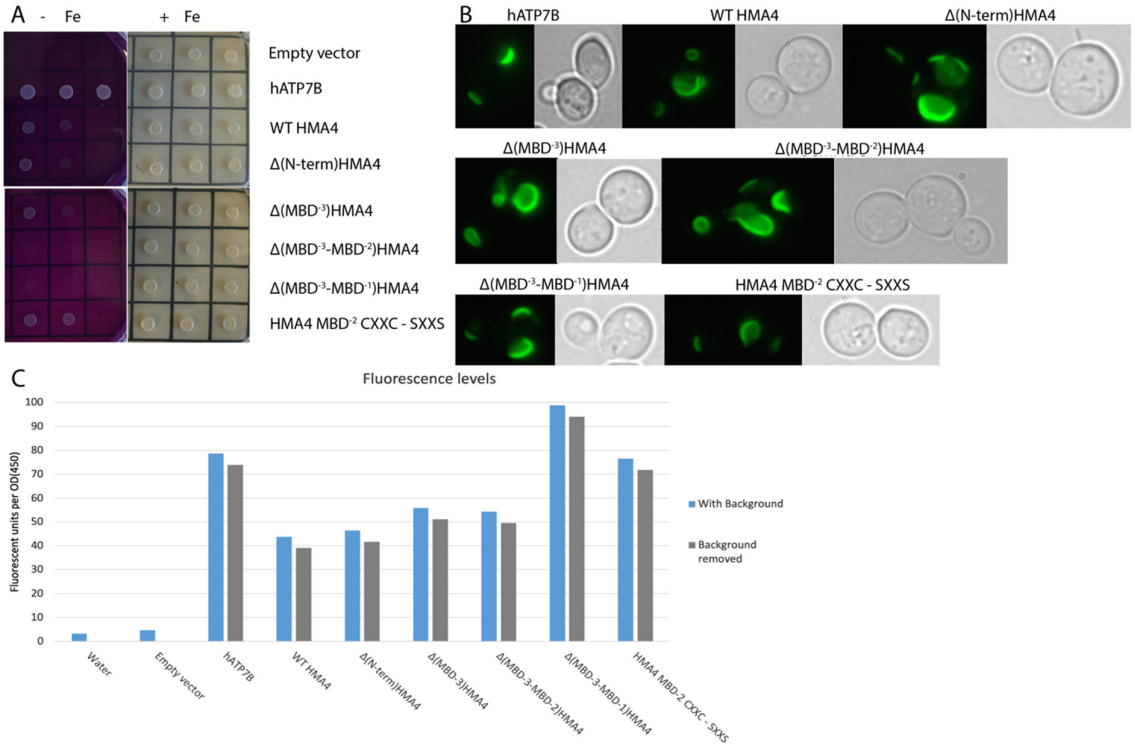

Supplementary figure 18: Complementation of Ccc2p deficient *Saccharomyces cerevisiae*. **A:** For assessing the function of P_{1B-1}-ATPases, the assay requires low iron levels (-Fe), as Ccc2p is essential for high-affinity iron uptake. Controls grown at normal iron levels (+Fe) are also shown. The indicated yeast strains were spotted at three different densities (from left to right; 5 µL 0.50 OD_{450}/mL; 5 µL 0.05 OD_{450}/mL; 5 µL 0.005 OD_{450}/mL). Plates were imaged after 72 hours. The assessed forms are empty vector (essentially the Ccc2p deficient *Saccharomyces cerevisiae* strain), hATP7B, WT HMA4 (wild-type HMA4), Δ(N-term)HMA4 (HMA4 lacking the N-terminal tail preceding MBD^{-3}), Δ(MBD^{-3})HMA4 (HMA4 lacking MBD^{-3} and preceding amino acids), Δ(MBD^{-3}-MBD^{-2})HMA4 (HMA4 lacking MBD^{-2} and all preceding parts), Δ(MBD^{-3}-MBD^{-1})HMA4 (HMA4 lacking MBD^{-1} and all preceding parts) and HMA4 MBD^{-2} CXXC - SXXS (HMA4 with the CXXC-motif of MBD^{-2} mutated to SXXS). **B:** Live cell bioimaging of yeast strain PAP6064 expressing C-terminally GFP tagged hATP7B or HMA4 variants. GFP tagged versions of hATP7B, WT HMA4 and HMA4 mutants show similar distinct localization in the *ccc2Δ* yeast strain, probably representing the late-Golgi compartment. Localization in the late-Golgi compartment is required for complementation of the high iron requirement of the *ccc2Δ* strain. Yeast cultures were inoculated at 30 ºC in standard minimal medium with galactose as sole carbon for 24 hours prior to live cell bioimaging. Left side of the figure shows GFP fluorescence while the right side shows the same cells imaged with differential interference contrast. **C:** GFP fluorescence levels detected in yeast strains expressing hATP7b or HMA4 (WT and different constructs).

Supplementary figure 19

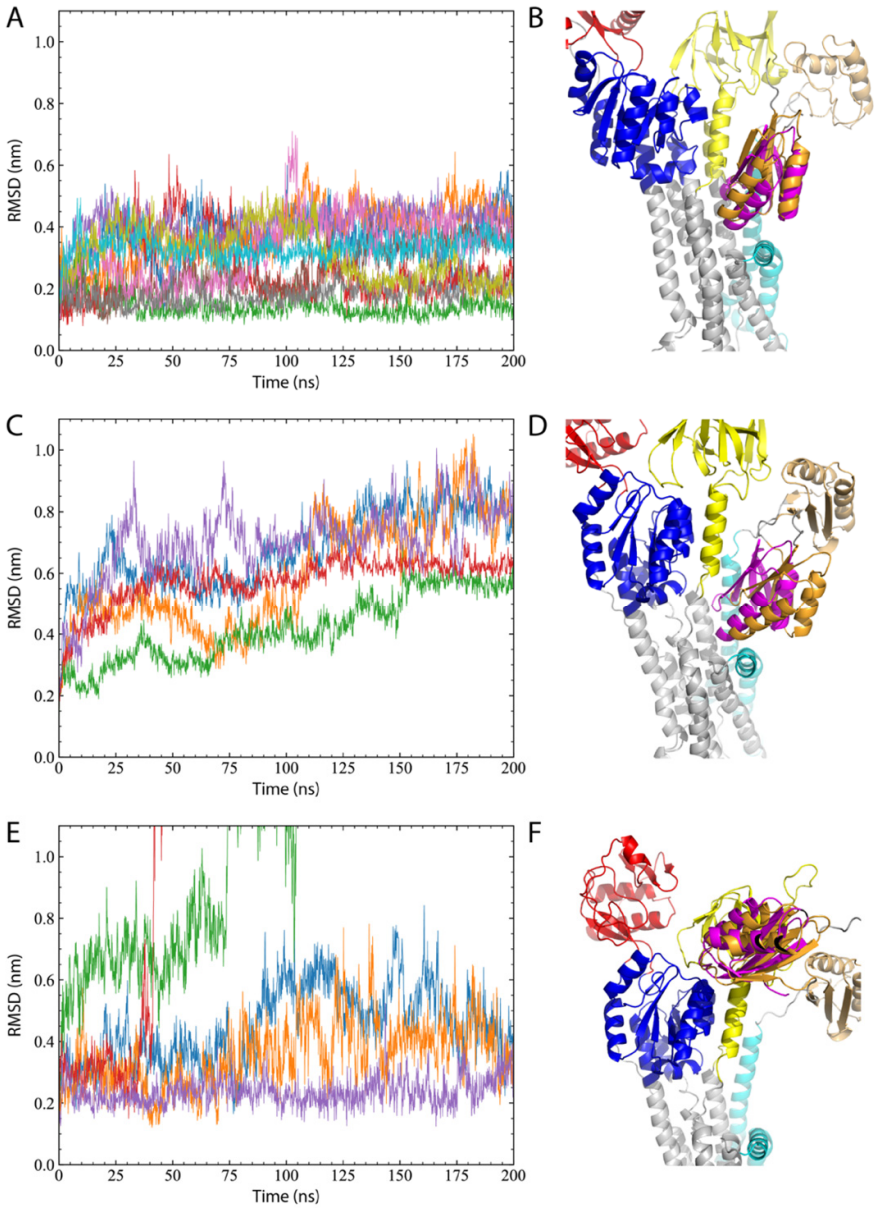

Supplementary figure 19: Molecular dynamics simulations. Stability of MBD^{-2} in the starting position. The RMSD traces of MBD^{-2} against starting structures with MBD^{-2} positioned as in AlphaFold model of HMA4 on MB' in simulations of **a,** the E1 and **c,** E2P state, respectively or **e,** with MBD^{-2} positioned as in the XtATP7B structures (in E2P simulations). The average RMSD with standard deviation for the three systems were 0.30±0.082 nm, 0.60±0.10 nm, 0.98±0.81 nm, respectively. **b,d,f,** shows the final structure of one of the higher RMSD trajectories three separate runs respectively. The M-domain is shown in grey, MA and MB in cyan, P-domain in blue, A-domain in yellow, N-domain in red and MBD^{-2} in orange. The starting position of MBD^{-2} is shown in magenta.

Supplementary figure 20

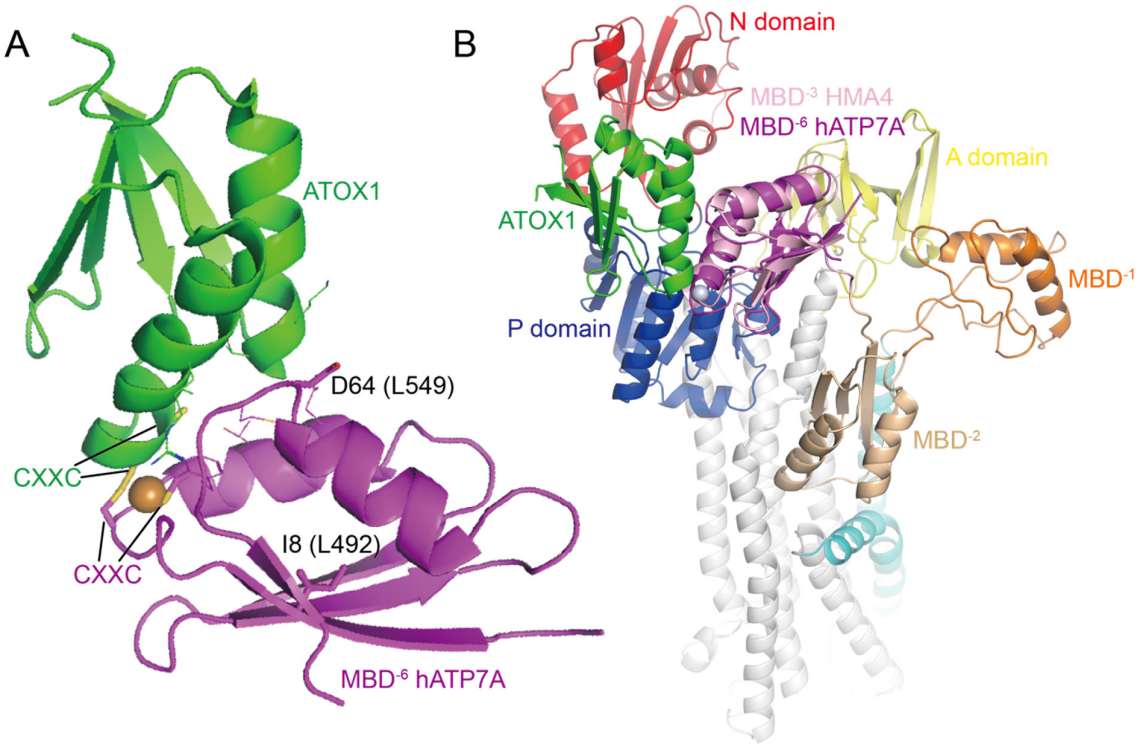

Supplementary figure 20: The complex between ATOX1 and a metal binding domain. A. Structure of ATOX1 in complex with MBD^{-6} of hATP7A (PDB-ID 2K1R). Side chains of residues located at the interaction interface are shown as lines, the CXXC motifs of each domain, as well as I8 and D64 of the MBD (correspond to L492 and L549 of hATP7B MBD^{-2}, respectively, are shown as sticks and labelled. **B.** Structural alignment of the ATOX1-MBD complex (PDB-ID 2K1R) and HMA4 (MD simulation of the E1 state). ATOX1-MBD is colored in green-purple, while HMA4 is colored as in Fig. 3c.

Supplementary figure 21

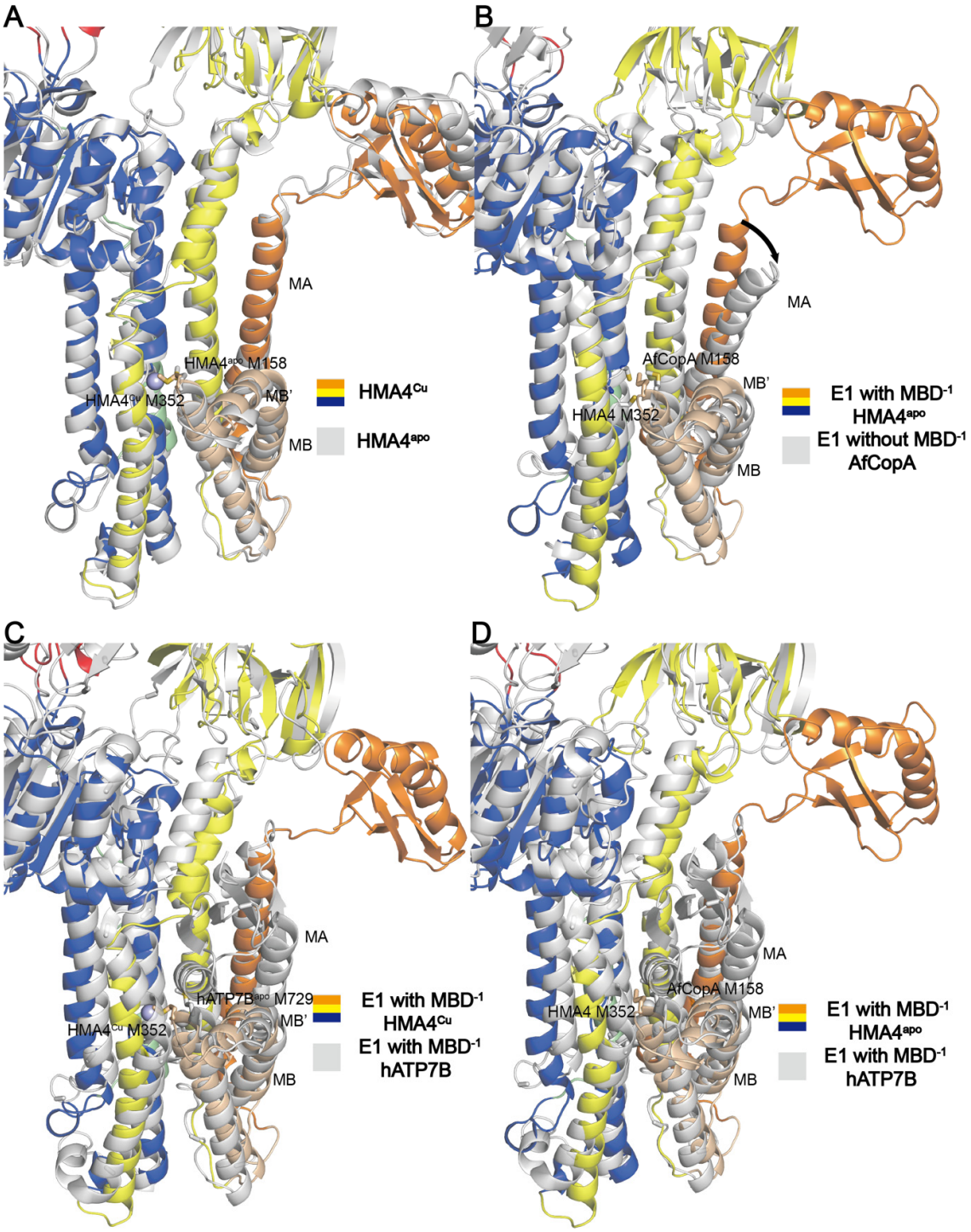

Supplementary figure 21: Structural comparisons of the determined HMA4 structures to other structures of P_{1B-1}-type ATPases.

Supplementary figure 22

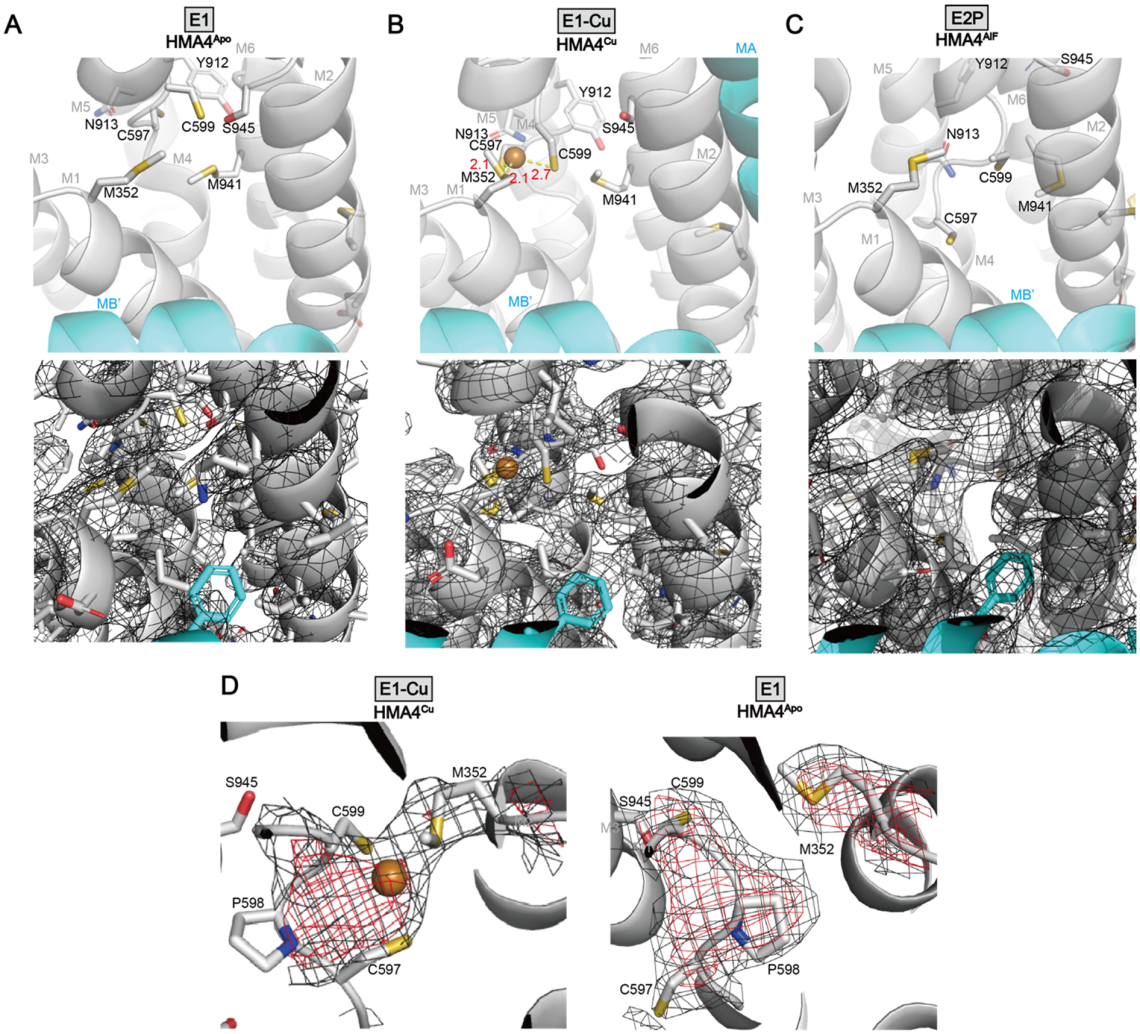

Supplementary figure 22: Densities of the copper binding site A-C, Top are replicates of Fig. 4A-C, with the bottom being the same views including electron density, showing $HMA4^{apo}$ (A), $HMA4^{Cu}$ (B) and $HMA4^{AlF}$ (C). **D.** Closeup of the copper binding site in $HMA4^{Cu}$ (left) and $HMA4^{apo}$ (right), with density shown at two different contour levels in red and black, respectively.

Supplementary table 1

	HMA4^{apo}	**HMA4^{Cu}**	**HMA4^{AlF}**	**HMA4^{BeF}**
	PDB: 8Q73	**PDB: 8Q74**	**PDB: 8Q75**	**PDB: 8Q76**
Data collection				
EM equipment	FEI Titan Krios	FEI Titan Krios	FEI Titan Krios	FEI Titan Krios
Voltage (kV)	300	300	300	300
Detecter	Gatan3	Gatan K3	Falcon 3	Falcon 3
Data collection mode	counting	counting	counting	counting
Pixle size (Å)	0.8617	0.8617	0.832	0.832
Energy filter	/	/	/	/
Electron dose (e^-/Å^2)	50	50	40	40
Defocus range (mm)	-1.2 ~ -2.6	-1.2 ~ -2.6	-1.2 ~ -2.6	-1.2 ~ -2.6
Data processing				
Software	cryosparc	cryosparc	cryosparc	cryosparc
Number of final used particles	104111	246045	184645	216398
Symmetry	C1	C1	C1	C1
Map resolution (Å)	3.58	3.68	3.20	3.29
Model refinement statistics				
Total built residues	779	784	774	774
Model-map-fit CC	0.73	0.80	0.84	0.82
R.m.s.d.				
bonds (Å)	0.004	0.004	0.004	0.003
angles (°)	0.916	1.004	0.982	0.739
Molprobity statistics				
Molprobity score	2.23	2.48	2.45	2.32
Ramachandran plot				
Favored (%)	86	83	86	87
Allowed (%)	13	16	12	12
Rotamer outliers (%)	1	1	2	0
Clash score	12	20	22	17
Average B-factor (Å^2)	289.03	291.94	213.03	227.17

Supplementary Table 1. Cryo-EM data collection, data processing and model building statistics.

Supplementary table 2

SERCA state	PDB ID	HMA4^{apo}	HMA4^{Cu}	HMA4^{AlF}	HMA4^{BeF}
		E1-apo	**E1-Cu**	**E2P-AlF**	**E2P-BeF**
E1	4H1W	9.5	8.0	12.1	12.2
[Ca]2 E1	2C9M	10.9	11.8	14.5	14.5
[Ca]2 E1	1SU4	11.2	11.5	13.2	13.0
[Ca]2 E1×ATP	3N8G	10.9	8.2	12.1	12.6
[Ca]2 E1P-ADP	1T5S	11.0	8.3	12.1	12.6
[Ca]2 E1-ADP:AlF4	1T5T	11.0	8.2	12.1	12.6
[Ca]2 E1P:ADP	3BA6	10.9	8.2	11.8	12.3
E2P	3B9B	10.9	13.8	4.8	4.6
E2-P	3N5K	11.2	13.6	3.9	4.0
E2:Pi	3FGO	11.3	13.5	4.1	4.1
E2	3NAL	9.8	10.6	5.5	5.7
P_{1B-1}-ATPases					
LpCopA^{AlF}	4BYG	8.3	10.1	1.8	1.6
LpCopA^{BeF}	4BBJ	7.3	8.8	2.9	2.8
AfCopA	7R0I	4.1	3.8	10.8	11.4
XtATP7B	7SI3	7.7	9.7	1.7	1.8
hATP7B	7XUM	4.6	3.8	11.3	11.6
AlphaFold models					
HMA4		3.3	3.4	7.3	7.1
hATP7B		3.5	3.4	7.5	7.5

M-domain	HMA4^{apo}	HMA4^{Cu}	HMA4^{AlF}	HMA4^{BeF}
HMA4^{apo}		0.9	3.0	3.3
HMA4^{Cu}	0.9		3.0	3.1
HMA4^{AlF}	3.0	3.0		0.6
HMA4^{BeF}	3.3	3.1	0.6	

Supplementary table 2: RMSDs of structural alignments of the determined HMA4 structures to the available structures of relevant P-type ATPases. Alignments were computed using super in Pymol and using the complete structures, except where indicated.

Supplementary table 3

System	Box dimensions	Nr atoms	Nr waters	Salt, concentration	Lipid composition
$E1^{apo}$	x: 120.2 Å y: 120.2 Å z: 156.5 Å	211,256	48,416	KCl: 0.15 M	POPC: 383
$E2P^{AlF}$	x: 120.2 Å y: 120.2 Å z: 160.3 Å	218,306	50,648	KCl: 0.15 M	POPC: 388
$E2P^{Xt}$	x: 120.1 Å y: 120.1 Å z: 171.9 Å	343,561	92,435	KCl: 0.15 M	POPC: 387

Supplementary table 3: Simulation system overview. Specifications of simulation box dimensions, numbers of atoms, water molecules, salt concentration, and lipid composition of the membrane.

Supplementary table 4

System	Trajectories (samples)	Mean CA RMSD (Å)	Stdev (Å)
$E1^{apo}$ MBD^{-2}	10	3.0	0.82
$E2P^{AlF}$ MBD^{-2}	5	5.9	1.0
$E2P^{Xt}$ MBD^{-2} all	5	9.8	8.1
$E2P^{Xt}$ MBD^{-2} stable	3	3.5	0.87

Supplementary table 4: Calculations of MBD^{-2} root mean square deviations (RMSD). RMSD for MBD^{-2} was calculated compared to the initial position. The mean and standard deviation values presented were calculated from the mean RMSD of each replica. "$E2P^{Xt}$ MBD^{-2} stable" refers to the three replicas where MBD^{-2} did not dissociate within the simulation time.

Uncropped SDS-PAGE gels - Supplementary figure 2

HMA4:

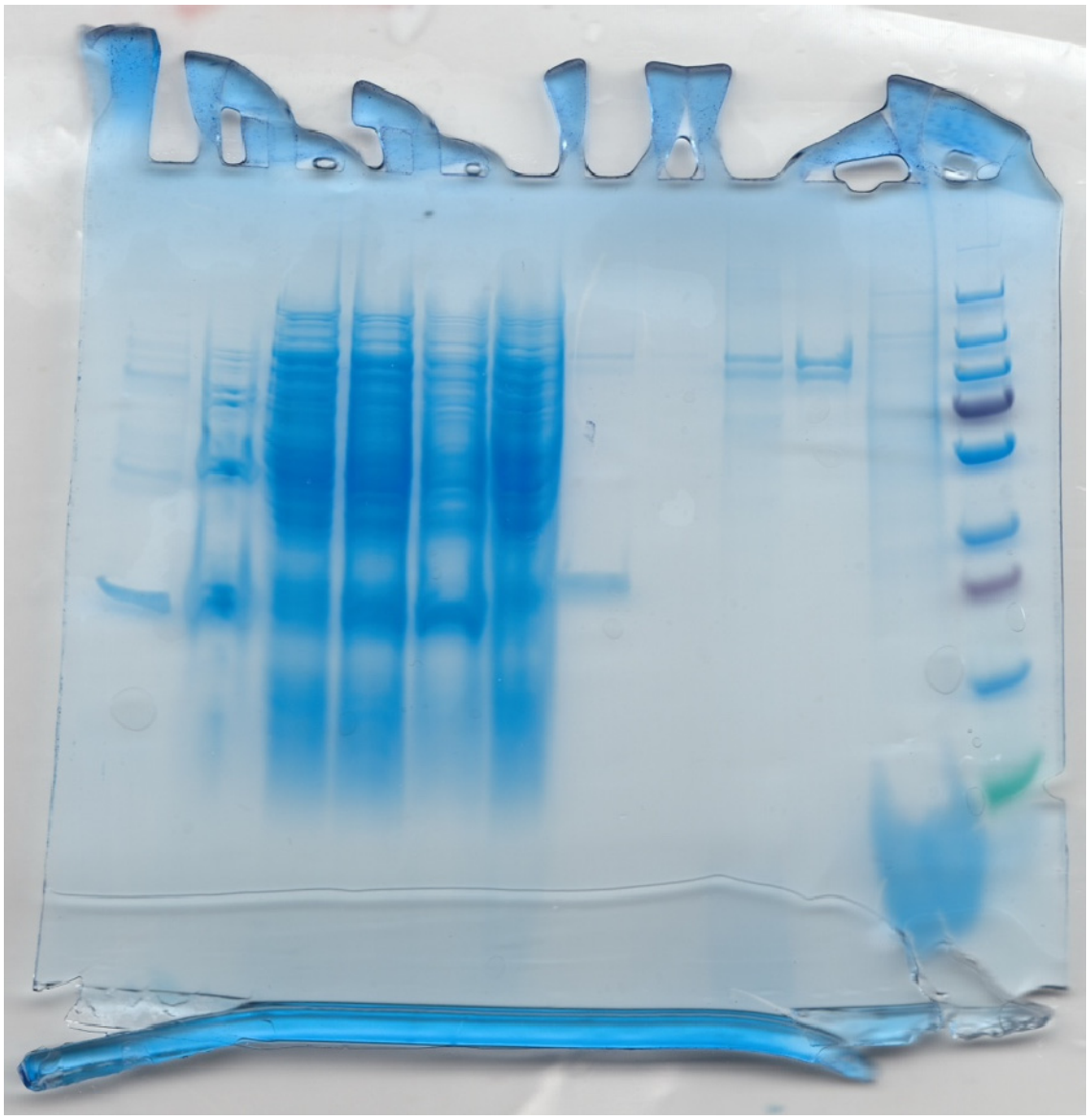

ATP7B: